

## Effects of Ambient Pressure on Fuel Sprays as Measured Using X-ray Absorption

C. F. Powell\*, Y. Yue, S.-K. Cheong, S. Narayanan, R. Cuenca, S. Ciatti, D. Shu and J. Wang  
 Center for Transportation Research and Advanced Photon Source  
 Argonne National Laboratory  
 Argonne, IL 60439 USA

### Introduction

Conventional diagnostics used in the study of high-pressure sprays are limited by the scattering of light from the many droplets surrounding the relatively dense core of the spray. Scattering is the dominant interaction between visible light and small droplets, and multiple scattering prevents quantitative data from being obtained, particularly in the regions of high droplet density near the nozzle. This limitation affects a number of modern spray analysis techniques, including diffraction techniques [1], exciplex fluorescence [2], and pulsed laser time-of-flight methods [3].

The x-ray absorption technique has been developed to overcome these limitations in the near-nozzle region. Over the past few years we have demonstrated the ability of the x-ray method to make quantitative, time-resolved measurements very near the nozzle [4-7]. However, these measurements were of limited use to the automotive spray community because they were performed in an ambient environment of room temperature and pressure.

In the past year we have fabricated a spray chamber suitable for x-ray absorption measurements in a pressurized ambient environment. This chamber features windows that can withstand the effects of pressure and x-ray damage while having minimal absorption of the low-energy x-rays. We present here our first series of measurements at increased ambient pressure using this new chamber. These measurements are the first step in what is anticipated to be a steady progression toward performing x-ray absorption measurements under realistic engine conditions. Measurements of sprays at high ambient pressure and temperature will allow injector designers to assess the impact of nozzle design on near-nozzle performance, and also provide quantitative, time-resolved data to spray modelers.

### Measurement Technique

The measurements were performed at the Advanced Photon Source at Argonne National Laboratory. The specialized source and x-ray optics at this facility can produce a very intense photon beam with a very narrow bandwidth of x-ray wavelengths. The monochromaticity of the x-ray beam results in a straightfor-

ward relationship between the measured x-ray intensity and the mass of fuel in the path of the beam, given by

$$\frac{I}{I_0} = \exp[-\mu_M M] \quad (1)$$

where  $I$  and  $I_0$  are the transmitted and incident x-ray intensities, respectively,  $M$  is the mass of fuel in the path of the x-ray beam, and  $\mu_M$  is the absorption constant which is measured in a standard cell.

A schematic of the experimental setup is shown in Figure 1. The x-ray energy of 6 keV was selected using a silicon double crystal monochromator. This energy was chosen to maximize the absorption by the fuel used in this work, which was a blend of diesel calibration fluid and a cerium additive. The beam was focussed to a small spot, then a beam size of  $50 \mu\text{m} \times 200 \mu\text{m}$  was defined by vertical and horizontal slits.

The injector was mounted perpendicular to the path of the x-ray beam, and could be moved in the plane perpendicular to the beam. This allowed the x-ray beam to probe different positions within the spray plume. For each set of spray conditions, measurements were made at approximately 1500 different positions on the spray's axial and transverse axes, with each position representing a single pixel of the final spray image. Combining all of these individual measurements allowed reconstruction of a two-dimensional projection of the spray onto a plane normal to the x-ray beam.

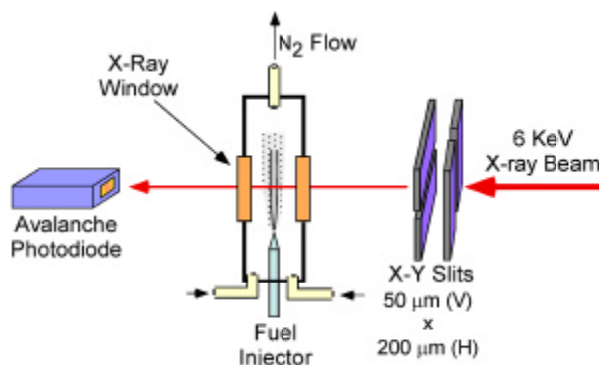


Figure 1. Schematic of the x-ray absorption setup.

\*Corresponding author

The x-ray intensity was monitored using an avalanche photodiode (APD). The APD had a time response faster than 1 ns, with an output proportional to the x-ray intensity. The APD output was recorded using a fast digitizing oscilloscope. Utilizing a fast detector and fast digitizer enabled us to measure the x-ray intensity as a function of time for the entire spray event. The oscilloscope was synchronized with both the x-ray beam and the firing of the fuel injector so that precise time measurements could be made. The measurements from 100 successive sprays (measured at a rate of 2.2 Hz) were averaged and the data was grouped into time bins of 3.68  $\mu$ s in order to improve signal to noise ratio. The measurement techniques are described in greater detail in [4].

These measurements were made using a common rail diesel injection system, the injection nozzle was a single-hole mini-sac type with an outlet diameter of about 180  $\mu$ m. The fuel/cerium blend had a density of 0.89 g/cm<sup>3</sup>, a viscosity of 1.0 cSt at 40° C, a surface tension of 30 Dynes/cm, and a temperature of 29° C for measurements at 500 bar and 38° C for measurements at 1000 bar. The sprays were directed into a chamber filled with nitrogen gas at room temperature, a continuous flow of gas (1 lpm) was maintained through the chamber to scavenge fuel vapors from previous sprays. For the work presented here, the effects of varying the ambient pressure in the spray chamber were explored. Measurements were made at spray chamber pressures of 1 and 2 bar (absolute). At each chamber pressure, measurements were made at injection pressures of 500 and 1000 bar. The duration of the current pulse to the injector was 400  $\mu$ s for all measurements.

## Results

Figure 2 shows the penetration of the leading edge of the spray as a function of time for 1 bar and 2 bar chamber pressures at an injection pressure of 1000 bar. The measured data are represented by the squares, the horizontal error bars reflect the uncertainty of the time measurement. The curves through the data are parametric fits of the form

$$S = C \cdot \Delta P^m t_{inj}^n \quad (2)$$

where  $S$  is the spray penetration,  $C$ ,  $m$ , and  $n$  are constants, and  $\Delta P$  and  $t_{inj}$  are the injection pressure and time after the start of injection, respectively. This parameterization of the penetration was described in [3] and does a good job reproducing the shape of the near-nozzle penetration, but is not expected to be suitable to model the penetration far from the nozzle.

Figure 3 shows the leading edge speeds for chamber pressures of 1 and 2 bar at injection pressures of 500 and 1000 bar. The speeds were calculated from the derivatives of the penetration curves, such as those shown in Figure 2. For both injection pressures, the

leading edge speeds near the nozzle are lower for the spray penetrating through the higher-pressure N<sub>2</sub> gas. The differences in speed that are evident near the nozzle diminish as the spray moves farther from the nozzle. At 500 bar injection pressure, the speeds are essentially the same at distances greater than 10mm. At 1000 bar, the sprays at the different ambient pressures reach equal speeds at a distance of about 5 mm from the nozzle. At this high injection pressure, the spray at 2 bar ambient pressure actually has a higher speed at distances beyond 6 mm. This effect is not yet understood, but we intend to investigate further utilizing visible light imaging.

Figure 4 shows images of the sprays reconstructed from the series of x-ray absorption measurements. Note that the colors of these images represent the mass of fuel in the x-ray beam normalized by the area of the beam. These units represent the two-dimensional density of the spray when projected onto a plane normal to the x-ray beam. The two images were measured 115  $\mu$ s after the start of injection at an injection pressure of 500 bar. The upper image was measured with an ambient pressure of 1 bar, the lower image at 2 bar. Comparing the two images clearly shows the speed difference between the two ambient pressures, with the spray into 1 bar showing a greater penetration at the same time after injection.

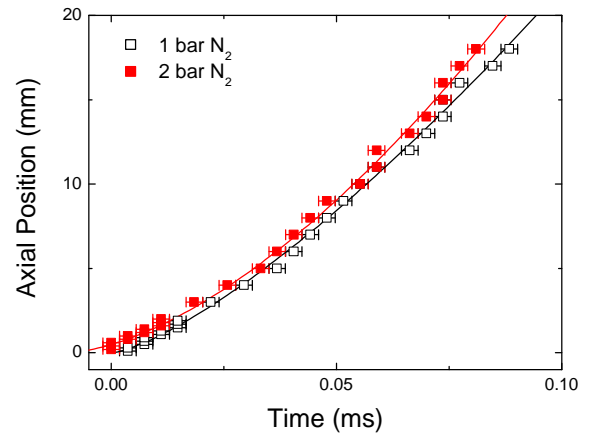


**Figure 2.** Axial position of the spray's leading edge as a function of time at an injection pressure of 1000 bar. The squares represent the measured spray penetration, the curves are a parameterization of the data as described in the text.

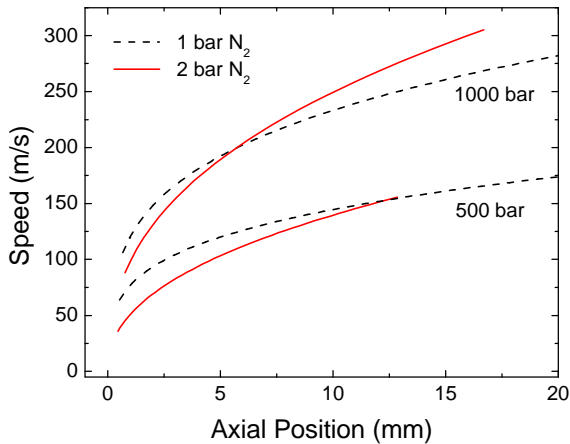


**Figure 3.** Leading edge speeds as a function of distance from the nozzle at injection pressures of 500 and 1000 bar. The dashed lines represent measurements at a spray chamber pressure of 1 bar, the solid lines are measurements at a chamber pressure of 2 bar.

The images also illustrate density differences in the spray which result from the change in ambient pressure. The highest density regions in both images are very near the nozzle, and the images show similar densities in this region of the spray. Farther from the nozzle, differences in density are apparent between the two images. The image at 1 bar pressure shows a low density region between 5 and 12 mm from the nozzle that is not apparent in the 2 bar image. This appears to result from the greater penetration of the leading edge at this ambient pressure. Since the total mass in the two images is the same, the deeper penetration results in a low-density region in this image.

The images also indicate significant differences in the density of the sprays at their leading edges. High density regions near the leading edges of the sprays are formed by collisions between the spray and the surrounding gases, resulting in a buildup of fuel near the leading edge and possibly coalescence of droplets. Such effects have been seen in studies with visible light, such as PDA measurements of relatively large droplets near the leading edge of the spray by Long *et al.* [8]. While both sprays show high density regions near their leading edges, the spray at two bar shows twice the density at the leading edge of the spray. The increased ambient pressure and the slower penetration lead to significantly higher densities in the two bar spray.

The transverse width of the sprays also has a dependence on the ambient pressure. In Figure 4, this is most clearly visible near the leading edges of the sprays. The two bar spray is much narrower than the one bar spray. This indicates that the spray expands in

the transverse direction more quickly at lower ambient pressures.

The lower image in Figure 4 shows features reminiscent of images presented by Lai *et al.* [9] which have been interpreted as evidence of buckling [10].

Figure 5 shows an image similar to that of Figure 4 but at an injection pressure of 1000 bar and 75  $\mu$ s after the start of injection. Note that at this higher injection pressure, the change in ambient pressure has little effect on the penetration length of the spray. However, the transverse width of the spray is again broader for the spray at lower ambient pressure.

The transverse width of the sprays is shown in detail in Figure 6. This figure plots the mass per unit area as a function of the transverse position at four different distances from the nozzle. All data in this figure were measured at 500 bar injection pressure and 115  $\mu$ s after the start of injection (the same conditions illustrated in Figure 4). The open squares represent the spray measured at 1 bar ambient pressure, the solid squares were measured at 2 bar. At a distance of 0.2 mm from the nozzle, the two sprays show nearly identical distributions. Farther from the nozzle both sprays broaden and the peak densities decrease, but the spray measured at 1 bar ambient pressure broadens more quickly, indicating a faster expansion in the transverse direction.

The transverse width of the spray shows similar behavior at 1000 bar injection pressure, though the data is not presented here. The transverse distributions are similar at 0.2 and 1 mm, but beyond 3 mm the spray injected into lower ambient pressure broadens more quickly.

## Conclusions

These measurements represent our first efforts to measure sprays at ambient pressures above atmospheric. We demonstrated that even a small change in the ambient pressure results in changes in the time-resolved structure of the spray, and that the x-ray technique is sensitive to these changes. At relatively low injection pressure the speed of the sprays near the nozzle is slowed significantly by the higher ambient pressure, but this effect decreases farther from the nozzle. At higher injection pressures the modest increase in ambient pressure has only a small effect on the speed of the spray. The expansion of the spray in the transverse direction is affected by the ambient pressure, with lower ambient pressure leading to greater transverse expansion. The ambient pressure also has a significant effect on the density distribution of the spray. While the densities are similar near the nozzle, the sprays at lower ambient pressure show a lower density at the leading edge and a very low density region just behind the leading edge.

We are continuing to move to higher ambient pressures and temperatures. We recently completed fabri-

cation of a redesigned pressure vessel for x-ray spray measurements and measured sprays at 5 bar ambient pressure in March 2003. By the end of the calendar year we expect to be able to measure sprays at 10 bar ambient pressure. There are a number of technical hurdles that must be overcome to measure sprays at pressures above 10 bar, but we expect to overcome these in the next year. Development of x-ray windows suitable for high temperature and pressure measurements is ongoing. We are nearing the final design of a rapid compression machine compatible with the x-ray absorption technique, and fabrication of this device will be complete by the end of 2003. With this device we will be able to make x-ray measurements of sprays at pressure and temperature conditions comparable to modern combustion engines. Such measurements will enable us to make even more significant contributions to the efforts of fuel system manufacturers and spray modelers.

#### Acknowledgments

This work and the use of the APS are supported by the U.S. Department of Energy, under contract W-31-109-Eng-38. The authors wish to acknowledge the support of Phillip Bohl and Johannes Schaller of Robert Bosch GmbH. The authors are also thankful to Patrick Fournier-Bidoz of Rhodia Terres Rares for providing the cerium additive. The assistance from Raj Sekar of ANL is very much appreciated. We also thank Tim Mooney and Kurt Goetze of ANL for their support during the experiments.

#### References

1. Coil, M.A., Farrell, P.V., *SAE* 950458 (1995).
2. Felton, P. G., Bracco, F. V., Bardsley, M. E. A., *SAE* 930870 (1993).
3. Galland, P. A., Liang, X., Wang, L., Breisacher, K., Liou, L., Ho, P., Alfano, R. R., *Proc. ASME Heat Transfer and Fluids Engineering Divisions* HTD-321: 585-588 (1995).
4. Powell, C.F., Yue, Y., Poola, R., and Wang, J., *J. Synchrotron Rad.* 7:356-360 (2000).
5. MacPhee, A. G., Tate, M. W., Powell, C. F., Yue, Y., Renzi, M. J., Ercan, A., Narayanan, S., Fontes, E., Walther, J., Schaller, J., Gruner, S. M., Wang, J., *Science* 295:1261-1263 (2002).
6. Yue, Y., Powell, C. F., Poola, R., Wang, J., Schaller, J. K., *Atomization and Sprays* 11:471-490 (2001).
7. Powell, C.F., Yue, Y., Liu, J., Cheong, S.-K., Narayanan, S., Wang, J., *Fifteenth Annual Conference on Liquid Atomization and Spray Systems*, Madison, WI, USA, May 2002, pp. 165-168.
8. Long, W. -Q., Ohtsuka, H., Obokata, T., *Jpn. Soc. Mech. Eng. Int.* 39:554-561 (1996).
9. Lai, M. C., Wang, T. -C. T., Xie, X., Han, J. -S., Henein, N., Schwarz, E., Bryzik, W., *SAE* 982542 (1998).
10. Smallwood, G. J., Gülder, Ö. L., *Atomization and Sprays* 10:355-386 (2000).

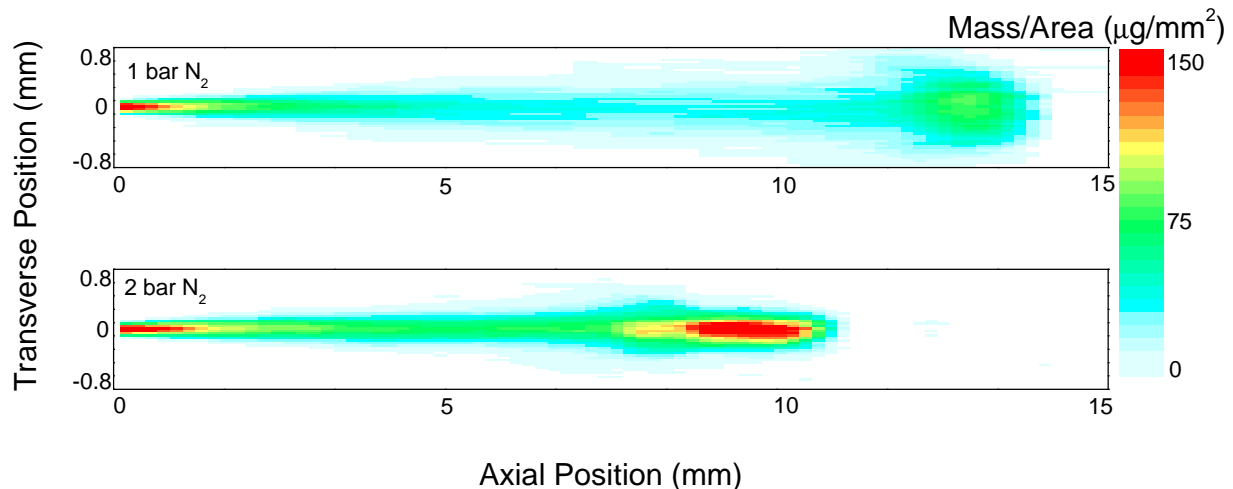


**Figure 4.** Images of the sprays reconstructed from the x-ray point measurement technique. The upper image was measured under 1 bar ambient conditions, the lower image was measured at 2 bar. Both images were measured 115  $\mu$ s after the start of injection at an injection pressure of 500 bar.

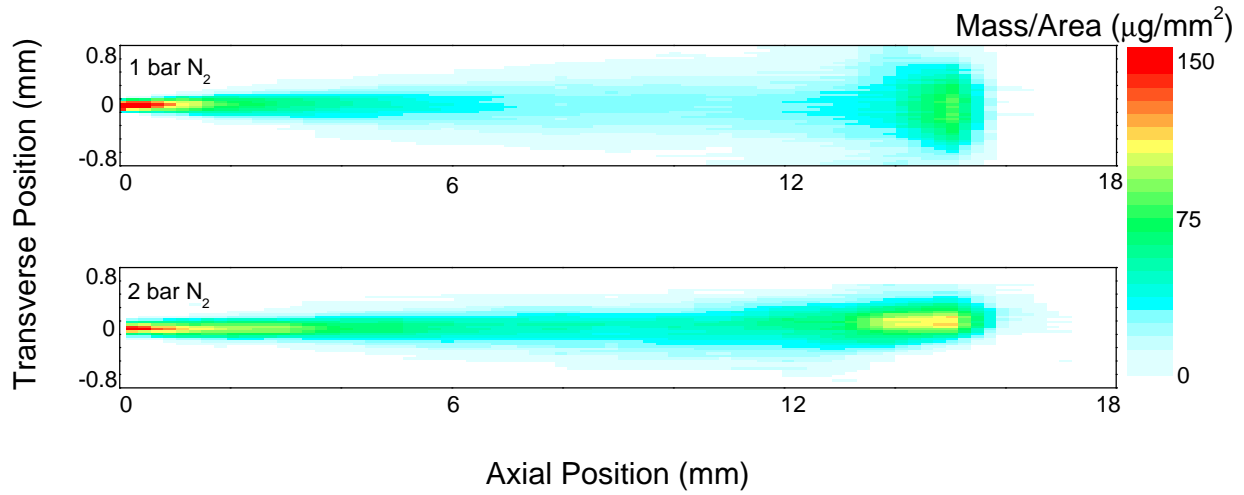


**Figure 5.** Images of the sprays reconstructed from the x-ray point measurement technique. The upper image was measured under 1 bar ambient conditions, the lower image was measured at 2 bar. Both images were measured 75  $\mu$ s after the start of injection at an injection pressure of 1000 bar.

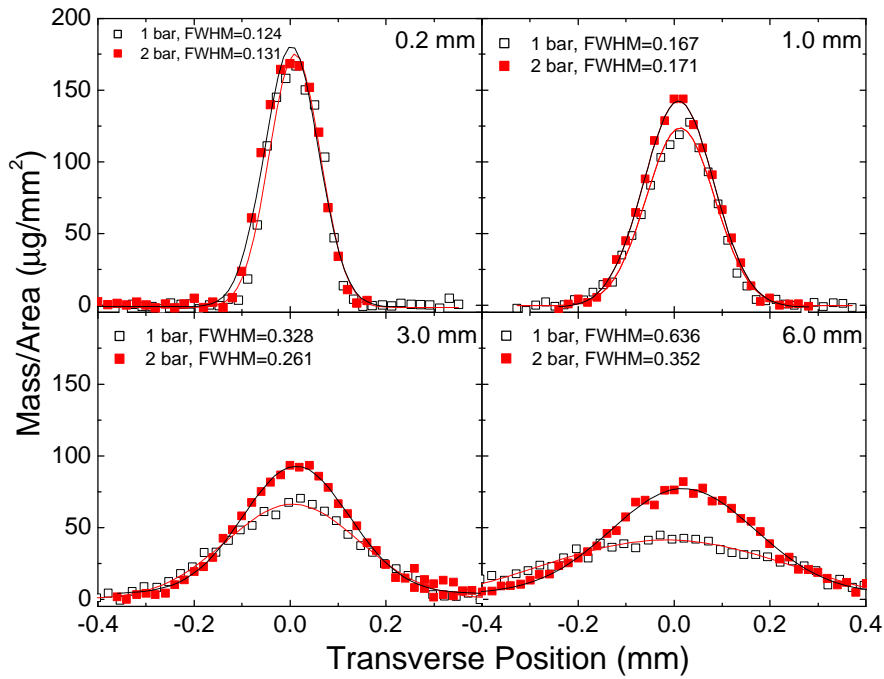


**Figure 6.** Mass distributions measured perpendicular to the spray axis at 0.2, 1.0, 3.0, and 6.0 mm from the nozzle. The solid squares represent measurements made at 1 bar injection chamber pressure, the open squares were measured at 2 bar. The curves are fits to the measured data, the full width at half maximum is given for each curve. All data were measured at an injection pressure of 500 bar 115  $\mu$ s after the start of injection.